J. Fluid Mech. (1998), *vol.* 363, *pp.* 281–300. Printed in the United Kingdom

The background flow method. Part 1. Constructive approach to bounds on energy dissipation

By ROLF NICODEMUS, S. GROSSMANN AND M. HOLTHAUS

Fachbereich Physik der Philipps-Universität, Renthof 6, D–35032 Marburg, Germany

(Received 11 August 1997 and in revised form 8 December 1997)

We present a numerical strategy that allows us to explore the full scope of the Doering–Constantin variational principle for computing rigorous upper bounds on energy dissipation in turbulent shear flow. The key is the reformulation of this principle's spectral constraint as a boundary value problem that can be solved efficiently for all Reynolds numbers of practical interest. We state results obtained for the plane Couette flow, and investigate in detail a simplified model problem that can serve as a definite guide for the application of the variational principle to other flows. The most notable findings are a bifurcation of the minimizing wavenumber and a pronounced minimum of the bound at intermediate Reynolds numbers, and a distinct asymptotic scaling of the optimized variational parameters.

1. Introduction

Mathematically rigorous results are scarce in the theory of turbulence. One of the few rigorous approaches arises from the attempt to derive inequalities for determining bounds on quantities that characterize turbulent flows. This approach had already reached a certain state of maturity 25 years ago (see Howard 1972); perhaps the most notable among the earlier contributions is the Optimum Theory developed by Busse (1970, 1978, 1996). For instance, this theory still gives for asymptotically high Reynolds numbers the best upper bound on the rate of energy dissipation in turbulent Couette flow that has been calculated so far.

The recent formulation by Doering and Constantin of a variational principle for bounding the energy dissipation rate in turbulent shear flow (Doering & Constantin 1994), channel flow (Constantin & Doering 1995), and convection (Doering & Constantin 1996) has therefore met with considerable interest. What is the actual scope of this new principle? Is it just a non-obvious reformulation of previous theories, or can one obtain further deep insights from it? These questions have already found a partial answer in the work of Kerswell (1997, 1998), who showed that the Doering–Constantin principle, if improved by a further variational parameter introduced by Nicodemus, Grossmann & Holthaus (1997*a*), yields precisely the same bound on the energy dissipation rate for the plane Couette flow, or the rate of heat transport in Rayleigh–Bénard convection, as the Optimum Theory. But still, these formal considerations do not yield the numerical values of the bounds. In order to fully explore the possibilities opened up by the Doering–Constantin principle, this principle has to be attacked head-on.

This is what we will do in the present work. Namely, we develop a numerical scheme that allows us to exploit the variational principle in the entire range from 'low' to 'high' Reynolds numbers, where the resulting bound shows a distinct asymptotic scaling behaviour. In addition to constructing a good approximate solution to the variational principle, we also analyse the mathematical structures underlying this solution.

In order to reach these goals we resort to a compromise. Although we will state results pertaining to the full unrestricted plane Couette flow, we will illustrate our techniques with the help of a simplified example, namely the Couette flow without spanwise degrees of freedom. This model problem exhibits virtually all salient features also encountered in the analysis of the unrestricted Couette problem, while allowing us to keep the technicalities within reasonable limits. On the other hand, this restriction makes possible a fairly detailed discussion of the crucial issues, which will then provide the starting points for the analytical theory developed in the follow-up paper, Part 2 (Nicodemus, Grossman & Holthaus 1998).

The present first part of our work is concerned with the numerical aspects of the variational principle. In § 2 we will state the principle for obtaining upper bounds on energy dissipation in plane Couette flow, and relate this principle to the works by Busse (1970, 1978, 1996) and Kerswell (1997, 1998). The main technical difficulty in evaluating the principle is caused by its spectral constraint, which seems to have prevented previous numerical work (Wick 1996; Doering & Hyman 1997) from reaching the asymptotic regime. In § 3 we show how to bring this spectral constraint into a form that can be dealt with efficiently even at asymptotically high Reynolds numbers, while § 4 describes the optimization procedure for a specific class of test functions. We then present our findings in § 5. The final § 6 offers a brief discussion, together with an overview of several results obtained up to now.

The aim of the present numerically oriented first part is twofold. On the one hand, we wish to provide a detailed example that can serve as a definite guideline when applying the extended Doering–Constantin principle to different, more complicated flows; on the other hand, we want to acquire some knowledge about how the principle works, and to collect clues for the analytical approach. The most important observation made here, namely a bifurcation of the minimizing wavenumber that determines the optimal upper bound on the dissipation rate, will be depicted in figure 7. In Part 2 of our work (Nicodemus *et al.* 1998) we will take up loose ends, and develop an analytical asymptotic theory of optimal upper bounds.

2. Variational principle for plane Couette flow

We consider the standard plane Couette geometry: an incompressible fluid with kinematic viscosity ν is confined between two infinitely extended rigid plates. The lower plate is at rest and coincides with the plane $z = 0$ of a Cartesian coordinate system, whereas the upper one at $z = h$ moves with constant velocity U in the positive x-direction. The dynamics of the fluid's velocity field $\boldsymbol{u}(\boldsymbol{x}, t)$ are governed by the equations

$$\partial_t \boldsymbol{u} + \boldsymbol{u} \cdot \nabla \boldsymbol{u} + \nabla p = \nu \nabla^2 \boldsymbol{u} \quad \text{(Navier–Stokes equations)}, \tag{2.1}$$

$$\nabla \cdot \boldsymbol{u} = 0 \quad \text{(incompressibility)}, \tag{2.2}$$

$$\boldsymbol{u}(x, y, 0, t) = \boldsymbol{0}, \quad \boldsymbol{u}(x, y, h, t) = U\hat{\boldsymbol{x}} \quad \text{(no-slip boundary conditions)}; \tag{2.3}$$

$\hat{\boldsymbol{x}}$ denotes the unit vector in x-direction. Periodic boundary conditions in the x- and y-directions are imposed on $\boldsymbol{u}$ and on the kinematic pressure p; the periodicity lengths

are L_x and L_y. Denoting the periodicity volume as $\Omega = L_x L_y h$, the time-averaged rate of energy (per mass) dissipated by the fluid is given by

$$\varepsilon_T \equiv \frac{1}{T}\int_0^T \mathrm{d}t\left\{\frac{\nu}{\Omega}\int_\Omega \mathrm{d}^3x\left[\sum_{i,j=x,y,z}(\partial_j u_i)^2\right]\right\}. \tag{2.4}$$

The objective of the background flow method is to calculate mathematically rigorous bounds on the long-time limit ε of ε_T,

$$\varepsilon \equiv \lim_{T\to\infty}\varepsilon_T, \tag{2.5}$$

or on the non-dimensionalized dissipation rate

$$c_\varepsilon(Re) \equiv \frac{\varepsilon}{U^3 h^{-1}}, \tag{2.6}$$

where $Re = Uh/\nu$ is the Reynolds number.

Energy stability theory, applied to the plane Couette flow, asserts (see Joseph 1976; Drazin & Reid 1981) that any initial deviation from the laminar solution $\boldsymbol{u}(\boldsymbol{x},t) = \left(Uz/h\right)\hat{\boldsymbol{x}}$ decays at least exponentially in time as long as the Reynolds number remains less than the energy stability limit $Re_{ES} \approx 82.65$. Thus,

$$c_\varepsilon(Re) = Re^{-1} \quad \text{for} \quad Re < Re_{ES}. \tag{2.7}$$

In addition, the laminar flow yields a rigorous lower bound $\underline{c_\varepsilon}$ for all Re, namely $c_\varepsilon(Re) \geqslant \underline{c_\varepsilon}(Re) \equiv Re^{-1}$ (Doering & Constantin 1994). Hence, the actual task is to formulate a theory for calculating *upper bounds* on c_ε for $Re \geqslant Re_{ES}$.

This task was tackled by Busse in the framework of his Optimum Theory (Busse 1970, 1978, 1996), which is based on a decomposition of the velocity field into a z-dependent plane-averaged flow and the accompanying fluctuations. This decomposition leads in a straightforward manner to a nonlinear Euler–Lagrange problem, for which Busse, using an asymptotic solution technique, found the so-called multi-α solutions. In this way he was able to derive an asymptotic upper bound on c_ε,

$$\lim_{Re\to\infty} c_\varepsilon(Re) \lesssim 0.010. \tag{2.8}$$

The right-hand side of (2.8) does not depend on the Reynolds number, so that the Optimum Theory is in accordance with the classical scaling behaviour (Kolmogorov 1941; Obukhov 1941; von Weizsäcker 1948; Heisenberg 1948; Onsager 1945; for a discussion of the connection between $c_\varepsilon(Re)$ and intermittency corrections see Grossmann 1995). As a consequence of the various approximations involved in the multi-α solutions, the numerical value of the constant is afflicted with some uncertainty†.

The approach recently pioneered by Doering & Constantin (1992, 1994) rests on a quite different decomposition of the velocity field. Instead of considering some kind of averaged mean flow, these authors revive an idea already put forward by Hopf (1941) and introduce an auxiliary stationary and divergence-free flow field $\boldsymbol{U}(\boldsymbol{x})$ that has to carry the boundary conditions of the physical flow: $\boldsymbol{U}(x,y,0) = \boldsymbol{0}$, $\boldsymbol{U}(x,y,h) = U\hat{\boldsymbol{x}}$, and $\boldsymbol{U}$ is assumed to be periodic in the x- and y-directions. Otherwise this auxiliary field, dubbed the *background flow*, can be chosen arbitrarily. The decomposition of

† According to F. H. Busse (private communication, 1996), this uncertainty may be of the order of 20%.

the flow field then reads

$$\boldsymbol{u}(\boldsymbol{x},t) = \boldsymbol{U}(\boldsymbol{x}) + \boldsymbol{v}(\boldsymbol{x},t), \tag{2.9}$$

where the divergence-free deviation $\boldsymbol{v}(\boldsymbol{x},t)$ from the background flow satisfies homogeneous boundary conditions for all instants $t \geqslant 0$, i.e. $\boldsymbol{v}(x,y,0,t) = \boldsymbol{v}(x,y,h,t) = \boldsymbol{0}$, and $\boldsymbol{v}$ is periodic in the x- and y-directions.

In the following we restrict ourselves to background flows that can be written in the form

$$\boldsymbol{U}(\boldsymbol{x}) \equiv U\phi(\zeta)\,\hat{\boldsymbol{x}}; \quad \phi(0) = 0, \quad \phi(1) = 1, \tag{2.10}$$

with a merely height-dependent profile function ϕ; the argument $\zeta \equiv z/h$ is the dimensionless coordinate in the cross-stream direction. We thus exclude background flows that have a spanwise structure. In addition, we require $\phi(\zeta) = 1 - \phi(1-\zeta)$, so that our background flow profiles reflect the symmetry of the geometry. Defining the profile functional

$$D\{\phi\} \equiv \int_0^1 \mathrm{d}\zeta\, \left[\phi'(\zeta)\right]^2 - 1 \tag{2.11}$$

and introducing the dimensionless balance parameter a, the variational principle for calculating the best upper bounds on $c_\varepsilon(Re)$ that the background flow method with the trial flows (2.10) has to offer stems from the inequality (see Nicodemus *et al.* 1997*a* for a detailed derivation)

$$c_\varepsilon(Re) \leqslant \inf_{\phi,a>1} \left\{ \left[1 + \frac{a^2}{4\,(a-1)} D\{\phi\} \right] Re^{-1} \right\}, \tag{2.12}$$

which is subject to a *spectral constraint*: ϕ and a have to be chosen such that all eigenvalues λ of the linear eigenvalue problem

$$\left.\begin{aligned} \lambda \boldsymbol{V} &= -2h^2\nabla^2\boldsymbol{V} + R\phi' \begin{pmatrix} 0 & 0 & 1 \\ 0 & 0 & 0 \\ 1 & 0 & 0 \end{pmatrix} \boldsymbol{V} + \nabla P, \\ 0 &= \nabla\cdot\boldsymbol{V}, \quad \boldsymbol{V} \text{ satisfies the homogeneous boundary conditions} \end{aligned}\right\} \tag{2.13}$$

for the stationary velocity fields $\boldsymbol{V}$ are positive. The balance parameter a enters into this eigenvalue problem via the rescaled Reynolds number

$$R \equiv \frac{a}{a-1} Re. \tag{2.14}$$

It is the presence of this balance parameter that distinguishes the variational principle (2.12) from the original principle first formulated by Doering & Constantin (1994). The balance parameter is necessary to ensure that the background flow method reproduces the known $1/Re$-behaviour of $c_\varepsilon(Re)$ up to the energy stability limit Re_{ES}, see Nicodemus *et al.* (1997*a*).

The above principle generalizes energy stability theory: following Doering & Constantin (1994) one can utilize the Navier–Stokes equations to relate ε_T to a functional of the deviations from the background flow, and then derive bounds on the long-time averaged dissipation rate by seeking this functional's extrema in an enlarged space of all stationary divergence-free fields satisfying the homogeneous boundary conditions. In this way one parallels directly the line of reasoning adopted in energy stability

theory (Joseph 1976; Drazin & Reid 1981). It is this enlargement of the space of admitted functions which effectuates that, even after optimization of the background flow $\boldsymbol{U}$, the background flow method can in general not yield the exact values of $c_\varepsilon(Re)$, but provides rigorous upper bounds $\overline{c_\varepsilon}(Re)$. Deviations of experimentally measured energy dissipation rates from these upper bounds thus characterize to what extent the actual solutions to the Navier–Stokes equations explore the enlarged function space.

Even though this background flow approach and Busse's Optimum Theory appear to be profoundly different at a first glance – somewhat arbitrary fields $\boldsymbol{U}$ here, genuine mean flows there – there exists an intriguing connection between them. By implementing the spectral constraint with the help of a Lagrange multiplier technique, one can transform the technical problem of optimizing the background flow into a nonlinear Euler–Lagrange problem quite similar to that appearing in Busse's work (Doering & Constantin 1994). Adopting this strategy, and applying Busse's multi-α technique to this new problem, Kerswell (1997) showed that the best bound obtainable with the background flow method coincides in the limit $Re \to \infty$ with the bound provided by the Optimum Theory. In his subsequent work, Kerswell (1998) was able to prove the equality of both bounds for all Re, without having to invoke multi-α solutions.

In spite of this formal identity of the bounds, there remain significant differences between the minimizing background flow and the mean flow occurring in Busse's theory. If the profile function ϕ is chosen optimally, the plane-averaged fluctuations around the background flow vanish (see Kerswell 1997) as do, by construction, the fluctuations around Busse's plane-averaged flow, but nevertheless in the limit $Re \to \infty$ this latter flow has a slope of $\frac{1}{4}U/h$ in the interior (Busse 1970, 1978, 1996), whereas the slope of the optimal profile ϕ vanishes.

From the computational viewpoint, a considerable advantage of the background flow method stems from its great flexibility. It can easily be adapted to other flow geometries (Wang 1997), or flows with non-stationary boundary conditions (Marchioro 1994), and for the purpose of constructing upper bounds on c_ε it is not necessary to know the optimal profile (or the optimal three-dimensional background flow) beforehand. Any profile ϕ of the required form, in combination with an arbitrary $a > 1$, gives rise to a maximal Reynolds number Re_c up to which the spectral constraint is fulfilled; by means of (2.12) one then obtains from that particular pair (ϕ, a) an exact upper bound on c_ε for all $Re < Re_c$.

The further treatment of the variational principle can be simplified considerably by observing that the optimization of the balance parameter a separates from the optimization of the profile function itself. Let us assume for the moment that we already have a method to evaluate the spectral constraint, i.e. to determine for an arbitrary ϕ that rescaled Reynolds number $R_c\{\phi\}$ where the lowest eigenvalue of (2.13) passes through zero. Then according to (2.12) this ϕ yields an upper bound on c_ε,

$$c_\varepsilon \leqslant \left[1 + \frac{a_{opt}^2}{4\left(a_{opt} - 1\right)} D\{\phi\}\right] Re^{-1} \quad \text{for} \quad 0 \leqslant Re < R_c\{\phi\}. \tag{2.15}$$

Taking into account the spectral constraint and (2.14), the optimization of a gives

$$a_{opt} = \begin{cases} 2 & \text{for} \quad 0 \leqslant Re < \frac{1}{2}R_c\{\phi\} \\ \dfrac{R_c\{\phi\}}{R_c\{\phi\} - Re} & \text{for} \quad \frac{1}{2}R_c\{\phi\} \leqslant Re < R_c\{\phi\}. \end{cases} \tag{2.16}$$

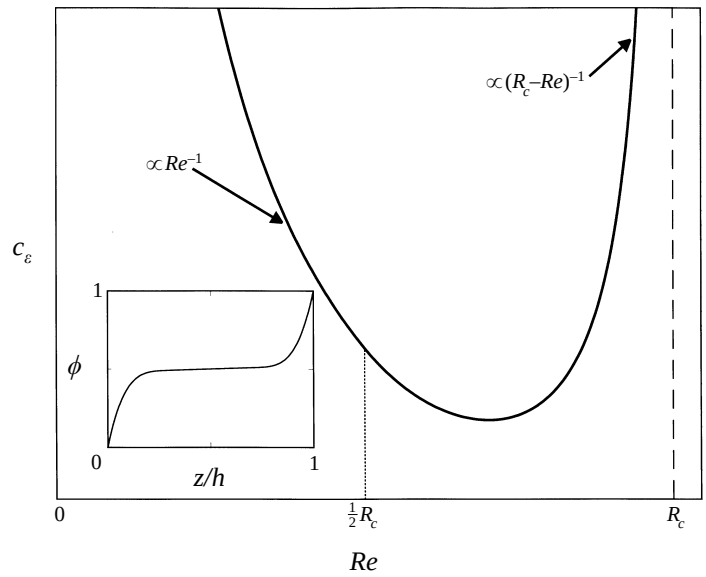

FIGURE 1. Graph of an upper bound on c_ε produced by the profile ϕ sketched in the inset.

Hence we obtain

$$c_\varepsilon \leqslant \begin{cases} [1 + D\{\phi\}]Re^{-1} & \text{for} \quad 0 \leqslant Re < \frac{1}{2}R_c\{\phi\} \\ \left[1 + \dfrac{D\{\phi\}R_c\{\phi\}^2}{4(R_c\{\phi\} - Re)Re}\right] Re^{-1} & \text{for} \quad \frac{1}{2}R_c\{\phi\} \leqslant Re < R_c\{\phi\}. \end{cases} \tag{2.17}$$

Figure 1 shows a typical graph of an upper bound (2.17) produced by a generic profile ϕ. Considered as a function of the Reynolds number, such an upper bound is continuous and even continuously differentiable at $Re = \frac{1}{2}R_c\{\phi\}$; it has exactly one minimum in the whole interval $0 \leqslant Re < R_c\{\phi\}$. This minimum appears in the upper half of this interval, i.e. for $\frac{1}{2}R_c\{\phi\} \leqslant Re < R_c\{\phi\}$.

The variation over a set of profile functions ϕ amounts to considering all their graphs in the (Re, c_ε)-plane; the optimal upper bound on $c_\varepsilon(Re)$ is then given by the lower envelope of these graphs. Provided the Re-dependence of this envelope is merely weak as compared with a graph originating from a particular profile ϕ, the only point that this ϕ can possibly contribute to the optimal bound $\overline{c_\varepsilon}(Re)$ – if any point at all – is its minimum point. The proviso obviously holds close to possible extrema of the bound, and in the limit $Re \to \infty$, where the bound becomes flat. Thus, we obtain a mapping from a profile ϕ to a point in the (Re, c_ε)-plane,

$$\phi \quad \mapsto \quad \left(Re_{min}\{\phi\}, \overline{c_\varepsilon}\left(Re_{min}\{\phi\}\right)\right); \tag{2.18}$$

here $\overline{c_\varepsilon}\left(Re_{min}\{\phi\}\right)$ denotes the right-hand side of (2.17) (for the profile ϕ considered) at $Re = Re_{min}\{\phi\}$. Minimizing the bound (2.17) with respect to Re, one sees that the Reynolds number $Re_{min}\{\phi\}$ of the minimum point can be expressed as

$$Re_{min}\{\phi\} = X_0\{\phi\}R_c\{\phi\}, \tag{2.19}$$

where $X_0\{\phi\}$ is the unique (real) zero of the cubic polynomial

$$x^3 - 2x^2 + \left(1 - \tfrac{3}{4}D\{\phi\}\right)x + \tfrac{1}{2}D\{\phi\} = 0 \tag{2.20}$$

that can be found between $\frac{1}{2}$ and 1, i.e. $\frac{1}{2} \leqslant X_0\{\phi\} < 1$.

The practical computation of upper bounds on the dissipation rate now hinges on the solution of two problems: one has to provide a method for calculating $R_c\{\phi\}$ for each given profile ϕ, i.e. for finding the rescaled Reynolds number (2.14) where the smallest eigenvalue of the eigenvalue problem (2.13) passes through zero, and one has to develop a procedure for minimizing $\overline{c_\varepsilon}(Re)$, i.e. for optimizing the profile by varying its parameters. These two issues will be taken up separately in the following two sections.

3. Implementation of the spectral constraint

In order to non-dimensionalize the problem, we now choose the gap width h as the unit of length. We denote the dimensionless quantities by the same symbols as their dimension-carrying counterparts. Thus, the eigenvectors $\boldsymbol{V}$ of (2.13) are henceforth regarded as dimensionless functions of the dimensionless variables x, y and z; the height variable z becomes equal to the variable ζ employed in (2.10).

Utilizing the periodic boundary conditions, the ansatz

$$\boldsymbol{V}(\boldsymbol{x}) = \boldsymbol{v}(z)\,\mathrm{e}^{\mathrm{i}(k_x x + k_y y)}, \quad P(\boldsymbol{x}) = p(z)\,\mathrm{e}^{\mathrm{i}(k_x x + k_y y)} \tag{3.1}$$

transforms the eigenvalue equation (2.13) into the system

$$\lambda v_x = -2\left(\partial_z^2 - \left(k_x^2 + k_y^2\right)\right)v_x + R\phi' v_z + \mathrm{i}k_x p, \tag{3.2}$$

$$\lambda v_y = -2\left(\partial_z^2 - \left(k_x^2 + k_y^2\right)\right)v_y + \mathrm{i}k_y p, \tag{3.3}$$

$$\lambda v_z = -2\left(\partial_z^2 - \left(k_x^2 + k_y^2\right)\right)v_z + R\phi' v_x + p', \tag{3.4}$$

$$0 = \mathrm{i}k_x v_x + \mathrm{i}k_y v_y + v_z' \tag{3.5}$$

with the boundary conditions

$$\boldsymbol{v}(0) = \boldsymbol{v}(1) = \boldsymbol{0}. \tag{3.6}$$

We consider only the non-trivial case $\left(k_x, k_y\right)^T \equiv \boldsymbol{k} \neq \boldsymbol{0}$ in the following.

It turns out that all methodical and conceptual aspects that characterize the solution procedure for the three-dimensional Couette flow appear even when the spanwise degrees of freedom are suppressed. However, in this simplified two-dimensional case the technical effort is reduced dramatically. To give but one example, the fourth-order eigenvalue problem that will appear in the analysis of the simplified flow becomes a sixth-order problem in the general case, so that the system of six coupled differential equations (3.13)–(3.18) then has to be replaced by a system of 20 equations. In order to elucidate the salient features of our approach without hiding essential points behind technicalities, we confine ourselves from now on to the case

$$v_y(z) = 0, \quad k_y = 0, \tag{3.7}$$

and leave the detailed discussion of the unrestricted, three-dimensional Couette flow to a separate publication (see Nicodemus, Grossmann & Holthaus 1997*b*).

Now the condition (3.5) allows us to express $v_x(z)$ in terms of $v_z'(z)$,

$$v_x(z) = \mathrm{i}\frac{v_z'(z)}{k_x}, \tag{3.8}$$

and to obtain an expression for $p(z)$ from (3.2),

$$p = \frac{1}{k_x^2}\left(2v_z''' - \left(2k_x^2 - \lambda\right)v_z'\right) + \mathrm{i}\frac{R}{k_x}\phi' v_z. \tag{3.9}$$

Inserting these expressions into (3.4) we arrive at a fourth-order equation for $v_z(z)$,

$$v_z^{(4)} - \tfrac{1}{2}\left(4k_x^2 - \lambda\right)v_z'' + \tfrac{1}{2}k_x^2\left(2k_x^2 - \lambda\right)v_z + \mathrm{i}k_x R\phi' v_z' + \tfrac{1}{2}\mathrm{i}k_x R\phi'' v_z = 0, \tag{3.10}$$

with the boundary conditions

$$v_z(0) = v_z'(0) = 0 \quad \text{and} \quad v_z(1) = v_z'(1) = 0. \tag{3.11}$$

For piecewise linear profiles ϕ, (3.10) becomes a system of equations with constant coefficients that can easily be solved (Orwoll 1994). However, for general curved profiles the equations (3.10) and (3.11) constitute an intricate eigenvalue problem, the solution of which cannot be obtained analytically. A numerical integration of (3.10) necessitates posing suitable initial conditions at a single boundary, say $z = 0$. Defining the four-vectors

$$\boldsymbol{V}_z(z) \equiv \left(v_z(z), v_z'(z), v_z''(z), v_z'''(z)\right)^T,$$

we consider the two fundamental solutions $\boldsymbol{V}_{z,1}$ and $\boldsymbol{V}_{z,2}$ to (3.10) that emerge from the initial conditions $\boldsymbol{V}_{z,1}(0) = (0,0,1,0)^T$ and $\boldsymbol{V}_{z,2}(0) = (0,0,0,1)^T$, respectively. The most general solution to (3.10) which satisfies the boundary condition (3.11) at $z = 0$ is then given by a superposition of these two fundamental solutions. The additional boundary condition at $z = 1$ yields the further constraint

$$\mathrm{Det}\begin{pmatrix} v_{z,1}(1) & v_{z,2}(1) \\ v_{z,1}'(1) & v_{z,2}'(1) \end{pmatrix} = v_{z,1}(1)\,v_{z,2}'(1) - v_{z,2}(1)\,v_{z,1}'(1) = 0. \tag{3.12}$$

Hence, when directly solving the boundary value problem (3.10), (3.11) by stepwise integration starting from $z = 0$, one has to adjust the parameters λ, k_x, and R (for given ϕ) such that (3.12) is fulfilled. However, (3.12) presents a severe numerical problem, since it involves the subtraction of two numbers of almost identical magnitude. An elegant way to overcome this difficulty is known as the *compound matrix method* in the literature (see e.g. Straughan 1992): instead of integrating a system of equations for v_z and its derivatives, one first reformulates the system in terms of determinants of the kind (3.12).

To this end, we define a new six-vector $\boldsymbol{y}(z)$. The components of this vector are the 2×2 minors of the 4×2 matrix that contains $\boldsymbol{V}_{z,1}$ as its first and $\boldsymbol{V}_{z,2}$ as its second column, i.e. of the solution matrix to the system considered above:

$$y_1 = v_{z,1}v_{z,2}' - v_{z,1}'v_{z,2}, \quad y_2 = v_{z,1}v_{z,2}'' - v_{z,1}''v_{z,2}, \quad y_3 = v_{z,1}v_{z,2}''' - v_{z,1}'''v_{z,2},$$
$$y_4 = v_{z,1}'v_{z,2}'' - v_{z,1}''v_{z,2}', \quad y_5 = v_{z,1}'v_{z,2}''' - v_{z,1}'''v_{z,2}', \quad y_6 = v_{z,1}''v_{z,2}''' - v_{z,1}'''v_{z,2}''.$$

The fourth-order equation (3.10) then leads to a system of six coupled equations,

$$y_1' = y_2, \tag{3.13}$$

$$y_2' = y_3 + y_4, \tag{3.14}$$

$$y_3' = y_5 + \tfrac{1}{2}\left(4k_x^2 - \lambda\right) y_2 - \mathrm{i}k_x R\phi' y_1, \tag{3.15}$$

$$y_4' = y_5, \tag{3.16}$$

$$y_5' = y_6 + \tfrac{1}{2}\left(4k_x^2 - \lambda\right) y_4 + \tfrac{1}{2}k_x^2\left(2k_x^2 - \lambda\right) y_1 + \mathrm{i}\tfrac{1}{2}k_x R\phi'' y_1, \tag{3.17}$$

$$y_6' = \tfrac{1}{2}k_x^2\left(2k_x^2 - \lambda\right) y_2 + \mathrm{i}k_x R\phi' y_4 + \mathrm{i}\tfrac{1}{2}k_x R\phi'' y_2. \tag{3.18}$$

The initial condition (3.11) at $z = 0$ yields

$$\boldsymbol{y}(0) = (0, 0, 0, 0, 0, 1)^T, \tag{3.19}$$

and (3.12) gives an additional boundary condition at $z = 1$,

$$y_1(1) = 0. \tag{3.20}$$

This kind of asymmetric boundary condition (3.19), (3.20) turns out to be very convenient for numerical analysis. An additional simplification can be obtained by reducing the complex system (3.13)–(3.18) to a real one: starting from the decomposition $\boldsymbol{y}(z) = \boldsymbol{f}(z) + \mathrm{i}k_x \boldsymbol{g}(z)$ with real vector functions $\boldsymbol{f}(z)$ and $\boldsymbol{g}(z)$, then taking $g_1(z) = 0$ successively produces

$$\left.\begin{aligned} &g_1 = 0, \qquad g_2 = 0, \qquad g_4 = -g_3, \qquad g_5 = \tfrac{1}{2}R\phi' f_1, \\ &g_6 = \tfrac{1}{2}\left(4k_x^2 - \lambda\right) g_3 + \tfrac{1}{2}R\phi' f_2, \qquad f_3 = \tfrac{1}{2}\left(4k_x^2 - \lambda\right) f_1 + f_4, \end{aligned}\right\} \tag{3.21}$$

where we have used $\phi'(z) \neq 0$. These equations are consistent with the initial condition (3.19), so that we arrive at a closed system of merely six real differential equations:

$$f_1' = f_2, \tag{3.22}$$

$$f_2' = \tfrac{1}{2}\left(4k_x^2 - \lambda\right) f_1 + 2f_4, \tag{3.23}$$

$$g_3' = -\tfrac{1}{2}R\phi' f_1, \tag{3.24}$$

$$f_4' = f_5, \tag{3.25}$$

$$f_5' = \tfrac{1}{2}k_x^2\left(2k_x^2 - \lambda\right) f_1 + \tfrac{1}{2}\left(4k_x^2 - \lambda\right) f_4 + f_6, \tag{3.26}$$

$$f_6' = \tfrac{1}{2}k_x^2\left(2k_x^2 - \lambda\right) f_2 + k_x^2 R\phi' g_3. \tag{3.27}$$

The corresponding initial conditions are

$$f_6(0) = 1, \quad \text{all other components vanish at } z = 0; \tag{3.28}$$

the condition at $z = 1$ reads

$$f_1(1) = 0. \tag{3.29}$$

For a given profile ϕ and a given set of parameters λ, k_x, and R, the unique solution to the initial value problem (3.22)–(3.28) together with the expressions (3.21) constitute the unique solution to the initial value problem (3.13)–(3.19). Thus, solving the eigenvalue problem (3.10), (3.11) becomes equivalent to solving the boundary value

problem (3.22)–(3.29). It seems that the system (3.22)–(3.27) captures the underlying symmetries in an optimal way, which is also reflected by the fact that it contains only the square of the wavenumber k_x. Hence, we can consider the absolute value $k \equiv |k_x|$ instead of k_x in the following.

For $\lambda \leqslant 2k^2$ and monotonic profiles with $\phi'(z) > 0$, we can understand intuitively how the initial value problem 'works': starting with f_6 (see (3.28)), the components f_5, f_4, f_2 and f_1 are driven successively. According to (3.24), g_3 is then driven with an opposite sign – the strength of the drive being regulated by the product $R\phi'$ – and acts back on f_6. If this feedback is so strong that f_6 itself becomes negative, the whole dynamics are repeated with opposite sign.

Obviously, the boundary condition (3.29) is fulfilled – an eigenvalue of (2.13) has been found – when a zero of $f_1(z)$ occurs at $z = 1$. As is clear from the above discussion, all eigenvalues of (2.13) will be positive for $R = 0$. Remember that our aim is to determine for any given profile ϕ that R-value $R_c\{\phi\}$ where the lowest eigenvalue passes through zero. We do so by keeping $\lambda = 0$ fixed when solving the system (3.22)–(3.27) numerically for a representative set of wavenumbers k, and monitor for each such k the dependence of $f_1(1)$ on R. In this way we identify the lowest value $R_0\{\phi\}(k)$ of the rescaled Reynolds number where the condition (3.29) is satisfied, i.e. the lowest zero of $f_1(1)$ as a function of R. The continuous dependence of the (discrete) eigenvalues of (2.13) on both the profile ϕ and the parameters R and k guarantees that this zero indeed corresponds, for the considered ϕ and k, to the passage of the lowest eigenvalue through zero.

The value $R_0\{\phi\}(k)$ is a functional of the profile ϕ and a function of the wavenumber k. Since the periodicity length L_x (and hence the wavenumber k_x) is a dummy variable in the actual problem, one has to determine the desired value $R_c\{\phi\}$ in a further step by minimizing over all k:

$$R_c\{\phi\} \equiv \min_{k>0} \{R_0\{\phi\}(k)\}\,. \tag{3.30}$$

Thus, for each profile ϕ the evaluation of the spectral constraint requires both the solution of a set of linear eigenvalue problems labelled by the wavenumber k, and a subsequent minimization. Figure 2 illustrates the k-dependence of $R_0\{\phi\}(k)$, for a generic ϕ. It should be noted that both steps, the identification of the first zero of the R-dependent function $f_1(1)$ for each k, and the minimization over k, can efficiently be implemented with the help of standard numerical routines.

4. Minimization of the upper bound

Having supplied a method for computing $R_c\{\phi\}$ for arbitrary profiles ϕ, and thus for finding their profile points (2.18), we can now turn to the actual minimization of the upper bound on $c_\varepsilon(Re)$.

We first have to specify the class of test profiles within which the variation is going to take place. To this end, we characterize these profiles ϕ by as few as possible and physically reasonable parameters. An educated guess for a useful class of test profiles can be made by recalling previous results: following Doering & Constantin (1992, 1994), one can verify the admissibility of a profile to the variational principle (2.12) by means of functional estimates. In this way the actual spectral constraint (2.13) is oversatisfied, so that one no longer obtains the best possible bounds, but with such an *over-restrictive profile constraint* the variational principle can be solved analytically (see Nicodemus *et al.* 1997*a*). For $Re > 20\sqrt{2}$ the resulting profiles consist

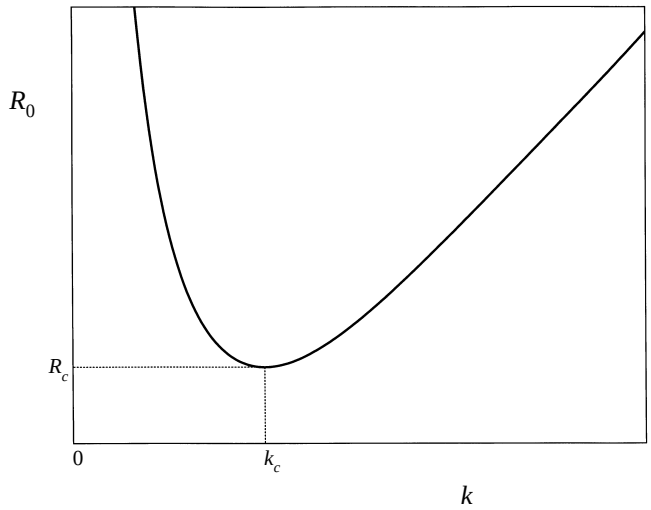

FIGURE 2. Behaviour of $R_0\{\phi\}(k)$ as a function of k for a generic profile ϕ, and the ensuing minimum $R_c\{\phi\}$ at the wavenumber k_c.

of parabolic boundary segments of thickness $\delta < \frac{1}{2}$ and a connecting line with zero slope in the interior, $\phi(z) = \frac{1}{2}$ for $\delta < z < 1-\delta$. However, remembering that the slope of Busse's (1970, 1978, 1996) mean flows does not vanish, whereas Kerswell (1997) obtained zero-slope profiles for $Re \to \infty$ when applying multi-α techniques to his Euler–Lagrange problem, it is clear that the slope p of the profiles in the interior should be one of the variational parameters.

Hence, a simple but promising class of test profiles consists of functions $\phi(z)$ with parabolic boundary segments of thickness δ $(0 < \delta < \frac{1}{2})$ that merge into a straight line with slope p $(0 < p \leqslant 1)$. We require that $\phi(z)$ be continuous and continuously differentiable at the merging points $z = \delta$ and $z = 1-\delta$. Our variational profiles are thus fully characterized by the two parameters δ and p,

$$\phi(z) = \begin{cases} (\delta p + (1-p))\, z/\delta - \frac{1}{2}(1-p)\left(z/\delta\right)^2 & \text{for} \quad 0 \leqslant z \leqslant \delta \\ \frac{1}{2}(1-p) + pz & \text{for} \quad \delta < z < 1-\delta \\ 1 - (\delta p + (1-p))\,(1-z)/\delta + \frac{1}{2}(1-p)\left((1-z)/\delta\right)^2 & \text{for} \quad 1-\delta \leqslant z \leqslant 1. \end{cases} \tag{4.1}$$

The profile functional (2.11) now becomes a function of δ and p,

$$D\{\phi\} = \left(\frac{2}{3\delta} - 1\right)(1-p)^2 \equiv \mathscr{D}(\delta, p)\,. \tag{4.2}$$

After $R_c\{\phi\} \equiv \mathscr{R}_c(\delta, p)$ has been computed numerically and the zero $X_0\{\phi\} \equiv \mathscr{X}_0(\delta, p)$ of the cubic polynomial (2.20) has been determined, each parameter pair (δ, p) can be mapped according to (2.18) to its profile point in the (Re, c_ε)-plane. With the help of a specifically adapted algorithm (for details, see Nicodemus 1997) we then construct the lower envelope of these points, i.e. the optimal upper bound on $c_\varepsilon(Re)$, for all Reynolds numbers of practical interest.

When performing this optimization in practice, one encounters some characteristic phenomena that accompany the increase of the Reynolds number. These phenomena

are not merely technical or numerical issues, but reflect the structure of the entire process that determines the optimal bound.

Above all, it has to be realized that the spectral constraint (2.13) acts as a sort of filter for the admissible profiles when Re, and hence R, becomes large. Regardless of the particular parametrization, the constraint singles out only those profiles that possess a large slope in the vicinity of the boundaries, but are comparatively flat in the interior. Intimately connected to this shape of the admissible profiles is the behaviour of $R_0\{\phi\}(k)$, considered as a function of the wavenumber k. Namely, the minimum structure of these functions changes at Reynolds numbers around 860: the single minimum occurring at lower Re splits into two separate minima. This fact forces us to keep track of two substantially different k-regimes when seeking the minima of $R_0\{\phi\}(k)$ for large Re, and to ensure that the numerically selected value $R_c\{\phi\}$ (cf. figure 2) actually corresponds to the global minimum. It will turn out that, as a consequence of the variational principle, both minima adopt the same value R_c, and that this balance is crucial for the scaling properties of the variational parameters and of $\overline{c_\varepsilon}(Re)$ itself.

The inevitable emergence of large k-values poses two problems for the numerical procedure. The first of these problems shows up in the behaviour of the zeros of $f_1(1)$ considered as a function of R. For a fixed boundary-layer-type profile ϕ and large wavenumbers, the lowest two zeros approach each other and finally coalesce in the limit $k \to \infty$. More generally, the zeros tend to get paired with increasing k. To give an example for the required numerical accuracy, we state the first four zeros for the parameters $\delta = 0.2$, $p = 0.1$, and $k_x/2\pi = 10$: the first and second zeros occur at $R_{0,1} = 5163.186\,160\,812\,7(1)$ and $R_{0,2} = 5163.186\,160\,812\,8(1)$, the third and fourth at $R_{0,3} = 9249.806\,408\,520\,3(1)$ and $R_{0,4} = 9249.806\,408\,520\,4(1)$; here and in the following the numbers in brackets give the uncertainty of the last digit. We are thus faced with the problem of distinguishing two closely spaced zeros, which can be overcome by first locating the minimum between those zeros and then using this minimum as starting value in a root-finding routine.

The second numerical problem stemming from large wavenumbers concerns the system of differential equations (3.22)–(3.27), with λ set to zero: it needs to be rescaled in order to reach the regime of large k. We define the new variables

$$q_1(z) \equiv k^4 f_1(z)\,\mathrm{e}^{-2kz}, \quad q_2(z) \equiv \tfrac{1}{2}k^3 f_2(z)\,\mathrm{e}^{-2kz}, \quad q_3(z) \equiv 2k^3 g_3(z)\,\mathrm{e}^{-2kz},$$
$$q_4(z) \equiv k^2 f_4(z)\,\mathrm{e}^{-2kz}, \quad q_5(z) \equiv \tfrac{1}{2}k f_5(z)\,\mathrm{e}^{-2kz}, \quad q_6(z) \equiv f_6(z)\,\mathrm{e}^{-2kz}.$$

The powers of k in this transformation are determined by the requirement that all components of the rescaled system be of the same order of magnitude even for large k; the common damping factor $\exp(-2kz)$ compensates an exponential growth of the components of the previous system (3.22)–(3.27). We will discuss in Part 2 why the value of the damping constant must be precisely $2k$.

Thus, the system of equations suitable for high-Re analysis reads

$$q_1' = 2k\,[-q_1 + q_2]\,, \tag{4.3}$$

$$q_2' = 2k[\tfrac{1}{2}q_1 - q_2 + \tfrac{1}{2}q_4], \tag{4.4}$$

$$q_3' = -2kq_3 - \frac{R}{k}\phi' q_1, \tag{4.5}$$

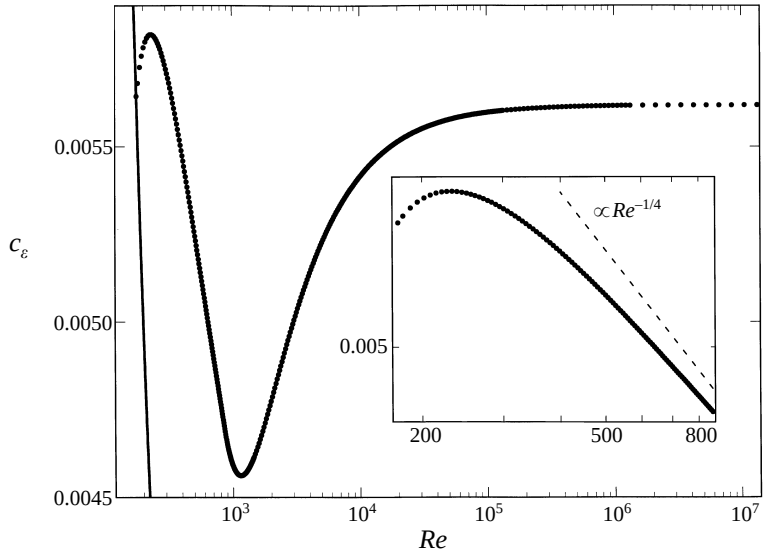

FIGURE 3. Bounds on c_ε. Points denote the optimal upper bound $\overline{c_\varepsilon}(Re)$ that can be obtained from the test profiles (4.1); the solid line at the left is the lower bound $\underline{c_\varepsilon}(Re) = Re^{-1}$. The inset shows the upper bound on a doubly logarithmic scale for Reynolds numbers between Re_{ES} and Re_B, see (5.5); the dashed line has the 'asymptotic' slope predicted by (5.7).

$$q_4' = 2k\,[-q_4 + q_5]\,, \tag{4.6}$$

$$q_5' = 2k[\tfrac{1}{4}q_1 + \tfrac{1}{2}q_4 - q_5 + \tfrac{1}{4}q_6], \tag{4.7}$$

$$q_6' = 2k\,[q_2 - q_6] + \frac{R}{2k}\phi' q_3\,; \tag{4.8}$$

its initial condition $\boldsymbol{q}(0) = (0,0,0,0,0,1)^T$ is supplemented by the boundary condition $q_1(1) = 0$. With the help of this system we have computed $\overline{c_\varepsilon}(Re)$ for Reynolds numbers up to 10^7, without encountering any kind of stability problem.

5. Results

Figure 3 shows the optimal upper bound on $c_\varepsilon(Re)$ that results from optimizing the test profiles (4.1), together with the lower bound $\underline{c_\varepsilon}(Re) = Re^{-1}$. The energy stability limit for the Couette flow with suppressed spanwise degrees of freedom is determined as

$$Re_{ES} = 177.214\,186\,80(1). \tag{5.1}$$

Below this Reynolds number the upper and lower bounds on c_ε coincide, see (2.7), so that

$$c_\varepsilon(Re_{ES}) = Re_{ES}^{-1} = 0.564\,288\,908\,27(4) \times 10^{-2}. \tag{5.2}$$

At Re_{ES} the upper bound resulting from the variational principle is continuous, but obviously not continuously differentiable; $\overline{c_\varepsilon}(Re)$ *increases* with Re for Reynolds numbers slightly above Re_{ES}. This is no artifact tied to our particular class of test profiles, but a generic feature. Even much more sophisticated parametrizations of the profiles yield the same qualitative picture in the vicinity of Re_{ES}.

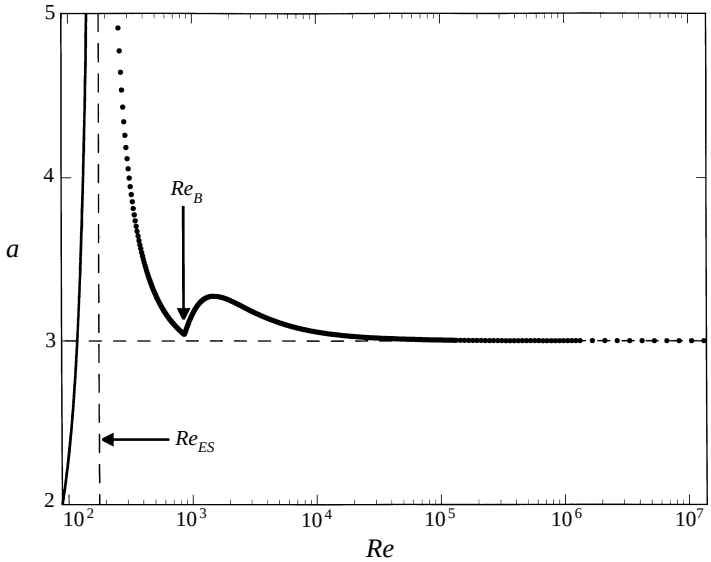

FIGURE 4. Balance parameter a for the optimal upper bound on c_ε as a function of the Reynolds number. For $Re < Re_{ES}$ this parameter is known analytically, see (2.16), and drawn as a solid line. For $Re > Re_{ES}$ the data points correspond to the bound depicted in figure 3. The vertical arrow marks the bifurcation number Re_B, see (5.5).

This interesting fact is related to the balance parameter a: the upper bound provided by the variational principle (2.12) with over-restrictive profile constraint, as calculated analytically by Nicodemus *et al.* (1997 *a*), shows a similar discontinuity of the derivative, albeit already at $Re = 16\sqrt{2}$, whereas there is no such discontinuity in the corresponding result obtained by Gebhardt *et al.* (1995) from the original Doering–Constantin principle, which implicitly fixes the balance parameter at the value $a = 2$. The Re-dependence of the optimal balance parameter that corresponds to the bound $\overline{c_\varepsilon}(Re)$ displayed in the previous figure is depicted in figure 4. Starting with the Doering–Constantin value $a = 2$ at $Re = \frac{1}{2}Re_{ES}$, it tends to infinity at $Re = Re_{ES}$. There is a kind of transition in the sense that the deviations $\boldsymbol{v}$ from the background flow $\boldsymbol{U}$ change their role abruptly at $Re = Re_{ES}$. Namely, for Reynolds numbers below Re_{ES} these deviations are fluctuations around a physically realizable flow, i.e. around a stationary solution to the equations of motion, but this is no longer the case for $Re > Re_{ES}$. The balance parameter then descends to the asymptotic value $a = 3$ which is known from analytical considerations (Nicodemus *et al.* 1997 *a*). It shows a kink at a Reynolds number Re_B, the significance of which will become obvious later.

A further characteristic feature of the optimal upper bound on c_ε shown in figure 3 is a distinct minimum. In the asymptotic limit $Re \to \infty$ the bound approaches the constant

$$\lim_{Re\to\infty} \overline{c_\varepsilon}(Re) = 0.561\,84(1) \times 10^{-2}. \tag{5.3}$$

In order to obtain more insight into the structure of the problem, we now consider the optimal profile parameters δ (the thickness of the boundary layers) and p (the profile slope in the interior) as functions of Re for $Re > Re_{ES}$. Figures 5 and 6 reveal

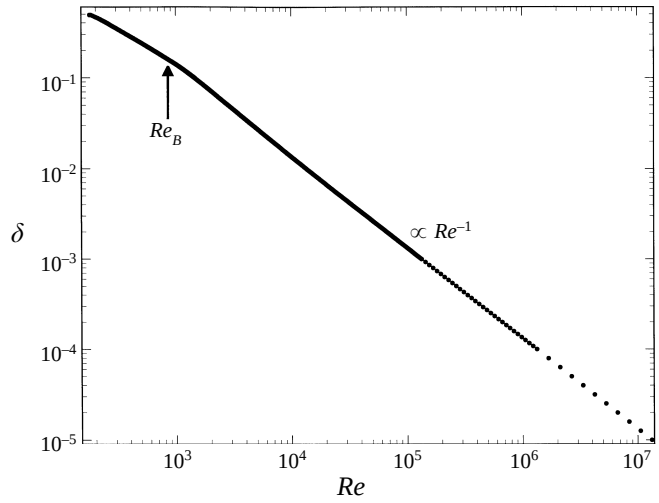

FIGURE 5. Optimal parameter δ, which denotes the thickness of the profiles' boundary layers, as function of the Reynolds number. The arrow marks the bifurcation number Re_B.

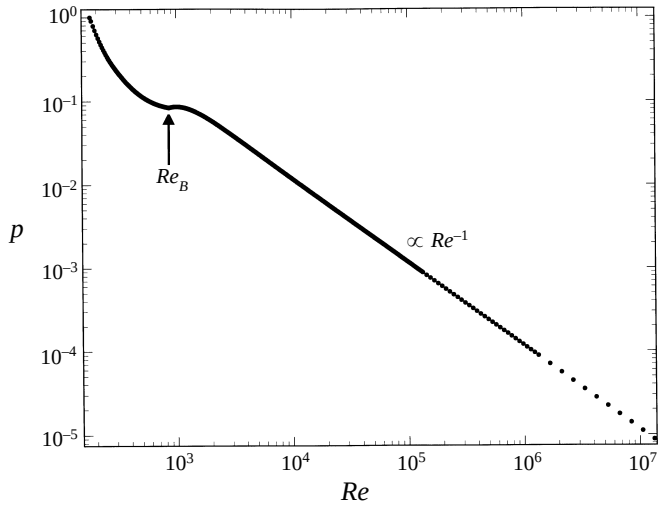

FIGURE 6. Optimal parameter p, which denotes the slope of the profiles in the interior, as function of the Reynolds number. The arrow again marks the bifurcation number Re_B.

that both parameters obey simple scaling laws in the asymptotic regime,

$$\delta \sim \alpha Re^{-1}, \quad p \sim \beta Re^{-1}; \tag{5.4}$$

with constants α and β. The accuracy of our method is emphasized by the fact that the numerically obtained optimal parameters do not show any noticeable scatter.

The most remarkable observation is that the Re-dependence of both parameters exhibits a pronounced change at

$$Re_B \approx 860, \tag{5.5}$$

as indicated by the arrows in figures 5 and 6. The width δ of the boundary layer alters its Re-dependence from an approximate $Re^{-3/4}$-law to the Re^{-1}-scaling. The

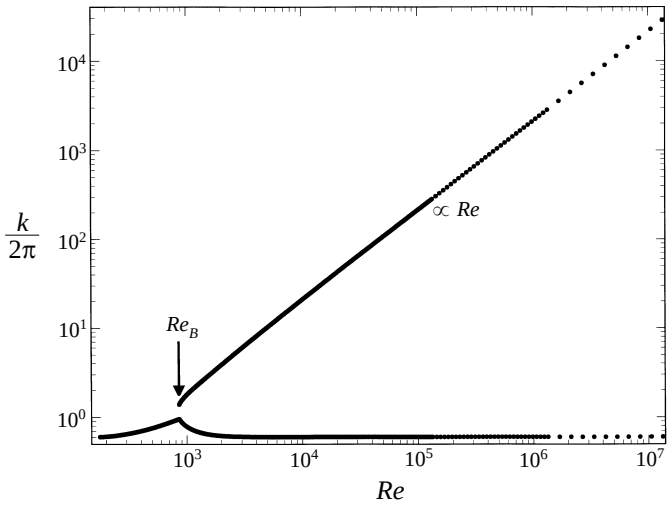

FIGURE 7. Plot of the wavenumber(s) k that minimize $R_0\{\phi\}(k)$, as function(s) of Re. The apparent discontinuity at the bifurcation point results from the finite Re-resolution.

change of the slope p is even more dramatic; p has a kink at Re_B. Likewise, the optimized balance parameter a has a kink, as shown in figure 4. These abrupt changes are caused by a phenomenon that has already been mentioned in § 4, namely the splitting of the single minimum of the functions $R_0\{\phi\}(k)$ into a double minimum. The variational problem possesses the property that for $Re > Re_B$ the optimal parameter p (for given δ) is uniquely determined by the condition that both minimal values of $R_0\{\phi\}(k)$ be equal. Expressed in mathematical terms: two eigenvalues of (2.13) characterized by two different wavenumbers pass through zero simultaneously. The resulting bifurcation of those wavenumbers that characterize the passage of the lowest eigenvalues of (2.13) through zero is featured in figure 7. For high Re the upper k-branch k_2 apparent in this figure scales proportionally to Re, whereas the lower branch k_1 approaches a constant value in the limit $Re \to \infty$. This asymptotic value coincides, within numerical accuracy, with the wavenumber k_{ES} that characterizes the zero eigenvalue at the energy stability limit:

$$\lim_{Re\to\infty} \frac{k_1}{2\pi} = \frac{k_{ES}}{2\pi} = 0.602\,677\,6(1). \tag{5.6}$$

This striking observation provides a key for an analytical asymptotic theory that will be elaborated in Part 2.

The splitting of a single minimum into a double minimum is a clear signature of the nonlinearity that is inherent in the optimization process as a whole. Even though the main technical problem of the background flow method consists in determining the value $R_0\{\phi\}(k)$ for each individual ϕ and k from a linear eigenvalue problem, it has to be kept in mind that both the minimization over the wavenumbers and the optimization of the profiles are essentially nonlinear operations. The bifurcation in k-space brought about by these nonlinearities entails strong consequences for the optimal upper bound on c_ε. If we take the scaling behaviour of δ for Reynolds numbers below the bifurcation ($\delta \propto Re^{-3/4}$) and set both the slope p and the balance parameter a to their asymptotic values ($p = 0$ and $a = 3$), we can simulate the asymptotic behaviour that

would prevail if there were no bifurcation. Then (2.15) and (4.2) immediately yield

$$\overline{c_\varepsilon} \sim \text{const.} \times Re^{-1/4}. \tag{5.7}$$

For comparison, the inset in figure 3 presents a doubly logarithmic plot of the upper bound in the interval $Re_{ES} \leqslant Re \leqslant Re_B$; it also depicts a straight line with the 'asymptotic' slope that is predicted by (5.7). The bifurcation takes place before this $Re^{-1/4}$-behaviour is fully developed, then leading to both the minimum of the upper bound and its actual asymptotic Re^0-scaling. But interestingly enough, the $Re^{-1/4}$-dependence of $\overline{c_\varepsilon}(Re)$ is exactly what one finds in Busse's theory for the case of a single boundary layer approximation (i.e. for a single-α solution; see Busse 1970, 1978 and Kerswell 1997), whereas the Re^0-scaling is equal to the scaling behaviour of Busse's asymptotic solution (2.8).

6. Discussion and outlook

After the pioneering works by Doering & Constantin (1992, 1994) and the following developments by Nicodemus *et al.* (1997 *a*) and Kerswell (1997) had already established the background flow method as a theoretical tool for computing rigorous upper bounds on quantities that characterize turbulent flows, the techniques developed in this paper constitute a constructive approach towards the actual solution of this method's variational principle. This approach is quite different from, and complementary to, the work of Kerswell (1997, 1998): there the variational problem was transformed into a nonlinear Euler–Lagrange type problem. If this problem could be solved exactly, it would give the best bounds that the background flow method can provide. However, an exact solution is exceedingly difficult; up to now only an approximate multi-α solution for asymptotically high Reynolds numbers is available. In contrast, we have divided the problem of calculating upper bounds into pieces that can be dealt with more easily, and deduce rigorous bounds for any value of Re. The price we have to pay is that the quality of our bounds depends on the choice of the test profiles.

The primary objective of this paper has been the solution procedure itself, rather than its application to a specific flow. The example problem studied here, a plane Couette flow with suppressed spanwise degrees of freedom, is of considerable interest since it illustrates in condensed form all essential steps that also occur in the analysis of physical problems, such as unrestricted shear flows or Rayleigh–Bénard heat convection.

In particular, the variational computation of upper bounds on the energy dissipation rate for the unrestricted, three-dimensional Couette flow directly parallels the simplified case. All characteristic features, from the occurrence of a bifurcation in k-space to the shape of the graph of the optimal upper bound, are met again, even though the corresponding equations are much more involved. We report in figure 8 our findings for this problem, see Nicodemus *et al.* (1997 *b*). This upper bound has been computed with the help of profiles that are parametrized in a more sophisticated manner than the profiles (4.1) considered up to now; the mathematical motivation for this improved parametrization will be given in Part 2. The upper bound for the unrestricted Couette flow separates from the lower one at

$$Re_{ES} = 82.650\,148\,87(1); \tag{6.1}$$

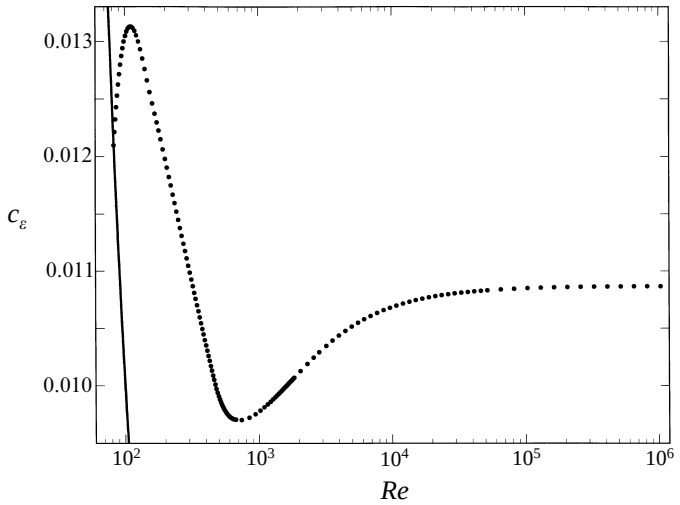

FIGURE 8. Bounds on c_ε for the unrestricted, three-dimensional Couette flow. Points denote the numerically computed variational upper bound $\overline{c_\varepsilon}(Re)$; the solid line on the left is the lower bound $\underline{c_\varepsilon}(Re) = Re^{-1}$.

correspondingly, the value of c_ε at the energy stability limit is given by

$$c_\varepsilon(Re_{ES}) = Re_{ES}^{-1} = 0.012\,099\,191\,758(2). \tag{6.2}$$

In the asymptotic limit the bound approaches the constant value

$$\lim_{Re\to\infty} \overline{c_\varepsilon}(Re) = 0.010\,87(1), \tag{6.3}$$

which is only minutely above (but within the uncertainty interval of) Busse's result (2.8). Hence, when backed by our techniques the background flow method competes in the asymptotic regime with the best other method known so far, and it is unrivalled in the important regime of intermediate Reynolds numbers.

The most significant step made in the present work is the identification of the mechanism that dictates the cross-over from intermediate to high Reynolds numbers and determines the asymptotic scaling behaviour of the optimal upper bounds, namely the bifurcation in k-space displayed in figure 7. In Part 2 we will develop an analytical asymptotic theory for our example problem. This will not only result in a detailed understanding of the bifurcation itself and of the scaling behaviour (5.4) of the optimized profile parameters, but also reveal which kind of further parameter is necessary in order to improve the numerically obtained asymptotic value of $\overline{c_\varepsilon}$.

Finally, we summarize in figure 9 the present status of research on the rigorous theory of upper bounds on the dimensionless dissipation rate c_ε for the turbulent plane Couette flow, including relevant experimental data for the energy dissipation rate. We recognize that replacing the over-restrictive profile constraint employed in earlier works (Doering & Constantin 1992, 1994; Gebhardt *et al.* 1995; Nicodemus *et al.* 1997*a*) by the actual spectral constraint (2.13) gives an improvement by about a factor of 8. But the gap that remains between the rigorous upper bounds and the experimentally measured dissipation rates still spans an order of magnitude. Moreover, the question whether the true dissipation rates exhibit a scaling correction in the limit $Re \to \infty$, perhaps a logarithmic correction as discussed by Doering & Constantin (1994), still remains to be answered.

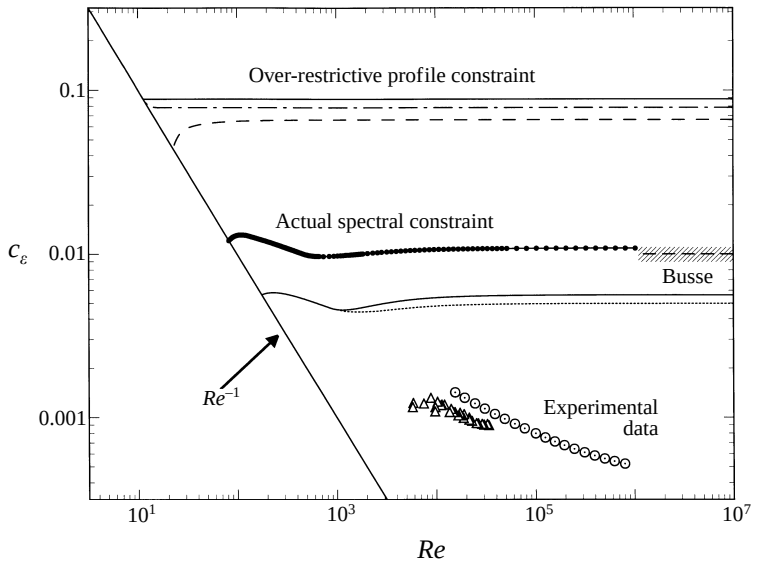

FIGURE 9. Comparison of bounds on $c_\varepsilon(Re)$. Solid slanted straight line: lower bound $c_\varepsilon(Re) = Re^{-1}$. Topmost horizontal solid line: upper bound obtained by Doering & Constantin (1992, 1994) with the help of an over-restrictive profile constraint and piecewise linear profiles; $\overline{c_\varepsilon}(Re) \approx 0.088$ for $Re > 11.32$. Dashed-dotted line: improved bound on $c_\varepsilon(Re)$ derived by Gebhardt *et al.* (1995) from the analytical solution of the Doering–Constantin principle with the over-restrictive constraint; $\overline{c_\varepsilon}(Re) \approx 0.079$ for $Re > 16.98$. Long-dashed line: further improvement due to the introduction of the balance parameter, see Nicodemus *et al.* (1997*a*); $\overline{c_\varepsilon}(Re) \to 0.066$. This bound is still calculated analytically utilizing the over-restrictive profile constraint. Heavy dots: upper bound for the unrestricted, three-dimensional plane Couette flow obtained by Nicodemus *et al.* (1997*b*) from the variational principle (2.12) with the actual spectral constraint (2.13), cf. figure 8; $\overline{c_\varepsilon}(Re) \to 0.010\,87(1)$. Following dashed line: asymptotic upper bound (2.8) derived by Busse (1970, 1978); $\overline{c_\varepsilon}(Re) \to 0.010(1)$. The shaded area denotes the estimated uncertainty of this bound. Solid line below: upper bound computed in this work for the restricted, two-dimensional Couette flow, cf. figure 3; $\overline{c_\varepsilon}(Re) \to 0.561\,84(1) \times 10^{-2}$. Dotted line: improvement obtained in Part 2 by optimizing the shape of the profiles' boundary segments, see (5.1) and (4.7) in Part 2; $\overline{c_\varepsilon}(Re) \to 0.498\,013\,3(1) \times 10^{-2}$. Triangles: experimental dissipation rates for the plane Couette flow measured by Reichardt (1959). Circles: experimental dissipation rates for the Taylor–Couette system with small gap as measured by Lathrop, Fineberg & Swinney (1992).

We would like to thank C. R. Doering for helpful comments. This work was supported by the Deutsche Forschungsgemeinschaft via the Sonderforschungsbereich 'Nichtlineare Dynamik', SFB 185, and by the German–Israeli-Foundation (GIF).

REFERENCES

BUSSE, F. H. 1970 Bounds for turbulent shear flow. *J. Fluid Mech.* **41**, 219–240.

BUSSE, F. H. 1978 The Optimum Theory of turbulence. *Adv. Appl. Mech.* **18**, 77–121.

BUSSE, F. H. 1996 Bounds for properties of complex systems. In *Nonlinear Physics of Complex Systems — Current Status and Future Trends* (ed. J. Parisi, S. C. Müller & W. Zimmermann). Lecture Notes in Physics, vol. 476, pp. 1–9. Springer.

CONSTANTIN, P. & DOERING, C. R. 1995 Variational bounds on energy dissipation in incompressible flows. II. Channel flow. *Phys. Rev.* E **51**, 3192–3198.

DOERING, C. R. & CONSTANTIN, P. 1992 Energy dissipation in shear driven turbulence. *Phys. Rev. Lett.* **69**, 1648–1651.

Doering, C. R. & Constantin, P. 1994 Variational bounds on energy dissipation in incompressible flows: shear flow. *Phys. Rev.* E **49**, 4087–4099.

Doering, C. R. & Constantin, P. 1996 Variational bounds on energy dissipation in incompressible flows. III. Convection. *Phys. Rev.* E **53**, 5957–5981.

Doering, C. R. & Hyman, J. M. 1997 Energy stability bounds on convective heat transport: numerical study. *Phys. Rev.* E **55**, 7775–7778.

Drazin, P. G. & Reid, W. H. 1981 *Hydrodynamic Stability*. Cambridge University Press.

Gebhardt, T., Grossmann, S., Holthaus, M. & Löhden, M. 1995 Rigorous bound on the plane-shear-flow dissipation rate. *Phys. Rev.* E **51**, 360–365.

Grossmann, S. 1995 Asymptotic dissipation rate in turbulence. *Phys. Rev.* E **51**, 6275–6277.

Heisenberg, W. 1948 Zur statistischen Theorie der Turbulenz. *Z. Phys.* **124**, 628–657.

Hopf, E. 1941 Ein allgemeiner Endlichkeitssatz der Hydrodynamik. *Math. Annalen* **117**, 764–775.

Howard, L. N. 1972 Bounds on flow quantities. *Ann. Rev. Fluid Mech.* **4**, 473–494.

Joseph, D. D. 1976 *Stability of Fluid Motions I & II*. Springer.

Kerswell, R. R. 1997 Variational bounds on shear-driven turbulence and turbulent Boussinesq convection. *Physica* D **100**, 355–376.

Kerswell, R. R. 1998 Unification of variational principles for turbulent flows: The background method of Doering–Constantin and Howard–Busse's mean-fluctuation formulation. *Physica D* (submitted)

Kolmogorov, A. N. 1941 The local structure of turbulence in incompressible viscous fluid for very large Reynolds numbers. *C. R. Acad. Nauk USSR* **30**, 301–305.

Lathrop, D. P., Fineberg, J. & Swinney, H. L. 1992 Turbulent flow between concentric rotating cylinders at large Reynolds number. *Phys. Rev. Lett.* **68**, 1515–1518.

Marchioro, C. 1994 Remark on the energy dissipation in shear driven turbulence. *Physica* D **74**, 395–398.

Nicodemus, R. 1997 Rigorous bounds on energy dissipation in turbulent shear flow. PhD thesis, Universität Marburg (http://archiv.ub.uni-marburg.de/diss/dissmain.html).

Nicodemus, R., Grossmann, S. & Holthaus, M. 1997*a* Improved variational principle for bounds on energy dissipation in turbulent shear flow. *Physica* D **101**, 178–190.

Nicodemus, R., Grossmann, S. & Holthaus, M. 1997*b* Variational bound on energy dissipation in plane Couette flow. *Phys. Rev.* E **56**, 6774–6786.

Nicodemus, R., Grossmann, S. & Holthaus, M. 1998 The background flow method. Part 2. Asymptomatic theory of dissipation bounds. *J. Fluid Mech.* **363**, 301–323.

Obukhov, A. M. 1941 On the distribution of energy in the spectrum of turbulent flow. *C. R. Acad. Nauk USSR* **32**, 22–24.

Onsager, L. 1945 The distribution of energy in turbulence. *Phys. Rev.* **68**, 285.

Orwoll, M. A. 1994 Rigorous drag bounds in turbulent shear flow. PhD thesis, Clarkson University.

Reichardt, H. 1959 Gesetzmäßigkeiten der geradlinigen turbulenten Couetteströmung. *Mitteilungen aus dem Max–Planck–Institut für Strömungsforschung*. Göttingen, No. 22.

Straughan, B. 1992 *The Energy Method, Stability, and Nonlinear Convection*. Springer.

Wang, X. 1997 Time averaged energy dissipation rate for shear driven flows in R^n. *Physica* D **99**, 555–563.

Weizsäcker, C. F. von 1948 Das Spektrum der Turbulenz bei großen Reynoldsschen Zahlen. *Z. Phys.* **124**, 614–627.

Wick, D. P. 1996 Energy dissipation in turbulent shear flows via an optimal background flow decomposition. PhD thesis, Clarkson University.